

Epitaxial Growth of Monolayer PdTe₂ and Patterned PtTe₂ by Direct Tellurization of Pd and Pt surfaces

Lina Liu,[†] Dmitry Zemlyanov^{*,○} and Yong P. Chen^{*,†,○,§,||,⊥}

[†]Department of Physics and Astronomy, Purdue University, West Lafayette, Indiana 47907, USA

[○]Birck Nanotechnology Center, Purdue University, West Lafayette, Indiana 47907, USA

[§]Purdue Quantum Science and Engineering Institute and School of Electrical and Computer Engineering, Purdue University, West Lafayette, Indiana 47907, USA

^{||}WPI-AIMR International Research Center on Materials Sciences, Tohoku University, Sendai 980-8577, Japan

[⊥]Institute of Physics and Astronomy and Villum Centers for Dirac Materials and for Hybrid Quantum Materials and Devices, Aarhus University, 8000 Aarhus-C, Denmark

ABSTRACT: Two-dimensional (2D) palladium ditelluride (PdTe₂) and platinum ditelluride (PtTe₂) are two Dirac semimetals which demonstrate fascinating quantum properties such as superconductivity, magnetism and topological order, illustrating promising applications in future nanoelectronics and optoelectronics. However, the synthesis of their monolayers is dramatically hindered by strong interlayer coupling and orbital hybridization. In this study, an efficient synthesis method for monolayer PdTe₂ and PtTe₂ is demonstrated. Taking advantages of the surface reaction, epitaxial growth of large-area and high quality monolayers of PdTe₂ and patterned PtTe₂ is achieved by direct tellurization of Pd(111) and Pt(111). A well-ordered (2×2) PtTe₂ pattern with Kagome lattice formed by Te vacancy arrays is successfully grown. Moreover, multilayer PtTe₂ can be also obtained and potential excitation of Dirac plasmons is observed. The simple and reliable growth procedure of monolayer PdTe₂ and patterned PtTe₂ gives unprecedented opportunities for investigating new quantum phenomena and facilitating practical applications in optoelectronics.

KEYWORDS: *two-dimensional materials, epitaxial growth, monolayer, defect, plasmons*

■ INTRODUCTION

Two-dimensional (2D) noble transition metal dichalcogenides (NTMDs) are a subgroup of 2D transition metal dichalcogenides (TMDCs) which exhibit drastically different properties from most widely studied TMDCs.¹ NTMDs demonstrate strong thickness-dependent band structures, high mobility, in-plane anisotropy and long-time air stability, offering exciting opportunities in nanoelectronics, optoelectronics and catalysis.²⁻⁹ For example, type II Dirac fermions with superconductivity in PdTe₂ have been shown, displaying strong possibilities for realizing the coexistence of superconductivity and topological states at 2D level for observing Majorana

fermions.¹⁰⁻¹³ For PtTe₂, excitations of 3D Dirac plasmons are observed, making it a promising candidate material for optoelectronic applications.¹⁴⁻¹⁶ On the other hand, both PdTe₂ and PtTe₂ show thickness-dependent band structures,¹⁷ which gives great opportunities to investigate their thickness-related electrical and optical properties. Therefore, it is highly desirable to achieve high-quality 2D PdTe₂ and PtTe₂ down to monolayers.

However, unlike common TMDCs, both PdTe₂ and PtTe₂ show strong interlayer interaction due to their specific electronic configurations (nearly full occupation of *d* orbitals and high hybridization of *p* orbitals),^{17, 18} which makes it challenging to obtain ultrathin 2D layers through “top-down” methods such as mechanical exfoliation. Very recently, PdTe₂ and PtTe₂ few layer flakes have been grown by molecular beam epitaxy (MBE) and chemical vapor deposition (CVD),¹⁹⁻²¹ demonstrating a promising “bottom-up” approach to synthesize monolayers. More interestingly, in another studied NTMD, platinum diselenide (PtSe₂), intrinsically patterned 1T/1H monolayer has been achieved during epitaxial growth by controlling concentration of defects,²² indicating a potential way to create 2D patterns of NTMDs with designed defect arrangements.

Here, we report the first synthesis of large-area PdTe₂ and PtTe₂ monolayer films by direct tellurization of Pd(111) and Pt(111) surfaces. Using a simple one-step approach, we obtained high-quality monolayer films confirmed by scanning tunneling microscopy (STM), X-ray photoelectron spectroscopy (XPS) and low-energy electron diffraction (LEED). In the case of PtTe₂, we obtained a (2×2) PtTe₂ pattern with Kagome lattice formed by well-ordered Te vacancies on the topmost layer. Multilayer PtTe₂ was also obtained by this method and potential excitation of Dirac plasmons was confirmed by high-resolution electron energy loss spectroscopy (HREELS). The reliable synthesis of monolayer PdTe₂ and patterned PtTe₂ will open new application opportunities for electronics and optoelectronics.

■ RESULTS AND DISCUSSION

PdTe₂ and PtTe₂ monolayers were grown by deposition of Te on Pd(111) and Pt(111) surfaces followed by annealing, respectively. The schematic cartoon of the process is shown in Figure 1. A large-area PdTe₂ monolayer film was obtained after annealing at 470 °C (Figure 2b). LEED shows hexagonal diffraction patterns, which confirms the (1×1) PdTe₂ structure and indicates high crystallinity over a large area of the as-grown film (insets of Figure 2b and Figure S1a). By manually changing positions of the

sample, LEED characterizations were carried out on different spots of the crystal. A series LEED results are shown in Figure S1. The diffraction patterns in all LEED images are nearly identical and displays one set of diffraction patterns, which indicates that the as-grown PdTe₂ film exhibits same crystalline orientation across the entire surface, proving the high quality and a large area of film with the size of several millimeters. The high-resolution STM image (Figure 2c) demonstrates the atomic structures of PdTe₂, which is hexagonal arrangements of Te atoms with an interatomic distance of 4.7 Å (Figure 2a and 2d). This number corresponds to ($\sqrt{3}\times\sqrt{3}$) lattice of Pd(111) ($\sqrt{3}\times 2.75=4.76$ Å), which indicates an in-plane lattice expansion of the as-grown PdTe₂ compared with bulk¹⁹ due to lattice match during epitaxial growth. In the case of PtTe₂, a monolayer film was obtained at low annealing temperature of 200 °C except for a few individual nanoparticles on the surface (Figure 2f). Unlike the regular (1×1) structure of PdTe₂, LEED displays hexagonal diffraction patterns of (2×2) PtTe₂ (inset of Figure 2f). A unique atomic arrangement is demonstrated (Figure 2e and 2g) in which holes form hexagonal arrays with the periodicity of 8.2 Å (Figure 2h), corresponding to (2×2) PtTe₂ Kagome lattice. These holes are defects of Te vacancies (V_{Te}) due to missing of Te atoms from the topmost layer. The size of the (2×2) PtTe₂ structure approximately matches three times of Pt(111) lattice (2×4.1 Å $\approx 3\times 2.77$ Å = 8.31 Å). Therefore, we can suppose that the generated Te vacancies rearrange into the (2×2) pattern, which is driven thermodynamically to match the lattice of underlying Pt(111) crystal. By counting the number of atoms in the STM images, stoichiometry of the (2×2) pattern is PtTe_{1.75} because one of four Te atoms on the topmost layer is missing. The (2×2) pattern demonstrates high thermal stability. Following annealing at 500 °C in ultrahigh vacuum (UHV), LEED patterns do not change and remain the (2×2) features (Figure S2a). The detailed STM image shows that the (2×2) PtTe₂ is still mainly intact although a few different vacancy defects are generated (Figure S2b-d). The (2×2) pattern is unique and only observed in PtTe₂ rather than PdTe₂. This phenomenon can be attributed to the higher energy of self-diffusion of atoms on Pt surface compared with Pd,²³ which leads to lower Pt-Te reactive abilities compared with Pd-Te system, resulting in losing Te easily and the formation of Te vacancies. The thickness of the as-grown films was calculated using XPS results (Figure 3). We used the XPS Thickness Solver tool from Nanohub²⁴ to calculate the layer thickness.

XPS thickness model is discussed in detail elsewhere.^{25, 26} This derivation follows the approach by Fadley.²⁷ The equation for the overlayer thickness, t , can be written as

$$\frac{N_l(\theta)}{N_s(\theta)} = \frac{\rho_l \times \frac{d\sigma_l}{d\Omega} \times A_l(E_l) \times \cos\theta}{\rho_s \times \frac{d\sigma_s}{d\Omega} \times A_s(E_s) \times \cos\theta} \times \frac{\left(1 - \exp\left(\frac{-t}{A_l(E_l) \times \cos\theta}\right)\right)}{\left(\exp\left(\frac{-t}{A_l(E_s) \times \cos\theta}\right)\right)} \quad (1)$$

Where $N_l(\theta)$ and $N_s(\theta)$ are the photoemission peak areas of the overlayer (l , Te 3d in our case) and substrate (s , Pd 3d or Pt 4f in our case) at the given photoemission angle, θ , with respect to the surface normal. Ω is the acceptance solid angle of the electron analyzer. ρ_l and ρ_s are the numbers of atoms per unit volume (density) for the overlayer and substrate. $(d\sigma_l/d\Omega)$ and $(d\sigma_s/d\Omega)$ are differential cross-section for the overlayer and substrate photoemission peak, which can be calculated from Scofield cross sections²⁸ and the Reilman asymmetry parameter.²⁹ $A_l(E_l)$ is the electron attenuation length (EAL) of overlayer electrons attenuated in the overlayer. $A_s(E_s)$ is the EAL of substrate electrons attenuated in the substrate. $A_l(E_s)$ is the EAL of substrate electrons attenuated in the overlayer. $A_l(E_l)$, $A_s(E_s)$ and $A_l(E_s)$ are calculated using NIST SRD-82.³⁰ Equation (1) can be solved numerically by using Nanohub.²⁴ To calibrate the thickness of a monolayer NTMD, we prepared monolayer PtSe₂, another NTMD which exhibits same atomic structures with PdTe₂ and PtTe₂, according to the protocol in the previous study.³¹ The thickness of PtSe₂ monolayer calculated using Equation (1) is equal to 2.26 Å. Therefore, this value is used as the reference of monolayer for our thickness calculation. The calculated thickness of epitaxially grown PdTe₂ and PtTe₂ in this study is 2.37 Å and 2.48 Å, respectively, corresponding to the thickness of monolayers. We point out that our thickness calculation based on XPS was crosschecked by transition electron microscopy (TEM) for TMDC materials such as MoS₂.²⁶

Chemical sensitivity of XPS characterizations also helps to confirm the formation of PdTe₂ and PtTe₂. After deposition at room temperature, the centroids of the Pd 3d_{5/2} and Pd 3d_{3/2} peaks are 335.6 eV and 340.9 eV, respectively, which shift towards higher binding energies (BEs) by 0.5 eV with respect to those of Pd(111) (Figure 3a and S3a), indicating the formation of Pd-Te chemical bonds right after deposition and giving evidence of the low reaction barrier between Pd and Te. After annealing, the Pd 3d_{5/2} peaks shift back to 335.1 eV. This is because the contribution of Pd(111) bulk dominates the XPS signal and the contribution of PdTe₂ monolayer is difficult to be separated. In contrast, Pt 4f peaks do not show significant shift before and after

annealing (Figure 3c and S3b), further indicating low reactive abilities between Pt and Te compared with Pd. The Te $3d_{5/2}$ and Te $3d_{3/2}$ peaks of PdTe₂ shift towards lower BEs by 0.2 eV after annealing, indicating the formation of PdTe₂ (Figure 3b). For both PdTe₂ and PtTe₂, the Te $3d_{5/2}$ and Te $3d_{3/2}$ peaks are 573.3 eV and 583.7 eV, respectively (Figure 3b and 3d), which are higher by ~0.5 eV than those of bulk materials.^{19, 21} This could be attributed to charge transfer between the epitaxial grown monolayers and substrates due to differences in work functions.^{32, 33}

The effect of annealing temperature was investigated. At low annealing temperature of 100 °C, the surfaces of PdTe₂ and PtTe₂ are not flat with islands (Figure S4a and 4a). The thickness of islands in PdTe₂ and PtTe₂ is 2.3 Å and 2.5 Å, corresponding to monoatomic steps of Pd(111) and Pt(111), respectively. The islands indicate breaking apart of monoatomic terraces and substantial mass-transport of materials during growth (Figure S4b), as well as non-thermodynamic equilibrium growth. In this case, the monolayer film behaves as a “carpet” covering the surface. Atomic structures of PdTe₂ can be resolved even after the low temperature annealing (inset of Figure S4a), further indicating a low reaction barrier between Pd and Te. However, in the atomic-resolution STM image of PtTe₂, coexistence of two structures with different atomic arrangements can be identified (labelled with “I” and “II” in Figure 4b). Structure I exhibits hexagonal atomic arrangements with the periodicity of 4.1 Å (Figure 4c and 4e), which corresponds to the (1×1) PtTe₂ lattice.³⁴ Typically, this structure is observed outside of the islands on the low areas. Structure II demonstrates the (2×2) PtTe₂ Kagome lattice (Figure 4d). LEED patterns display bright (1×1) and weak (2×2) diffraction spots, proving the coexistence of the two structures across a large surface area (inset of Figure 4b). Compared with the complete (2×2) pattern obtained under 200 °C, the emergence of regular (1×1) lattice of PtTe₂ at 100 °C is because more Te remains on the surface at low temperature. This phenomenon indicates that the amount of Te can play a significant role in the epitaxial growth of monolayer PtTe₂.

Therefore, we applied this method to grow PtTe₂ multilayers by increasing the deposited amount of Te (Figure 5a). Thickness calculated based on XPS results is 10.5 Å, corresponding to four layers approximately. As shown in Figure S5, the Pt $4f_{7/2}$ and $4f_{5/2}$ peaks of Pt are 71.6 eV and 74.9 eV, respectively, which shift to higher regions by 0.4 eV. Meanwhile, the Te $3d_{5/2}$ and $3d_{3/2}$ peaks shift to lower regions by 0.5 eV, resulting in doublet peaks at 572.8 eV and 583.2 eV. The binding energies of Pt and Te

confirm the formation of PtTe₂.²¹ According to the high-resolution STM image (Figure 5b), atomic structures were observed with the periodicity of 4.1 Å, corresponding to the lattice constant of PtTe₂.³⁴ LEED results show typical (1×1) diffraction patterns (inset of Figure 5a), indicating high crystallinity across a large surface area. Notably, potential excitation of Dirac plasmons of the multilayer PtTe₂ was observed at the energy of 0.4 eV by high-resolution electron energy loss spectroscopy (HREELS) (Figure 5c), which is close to the energy observed in PtTe₂ bulk crystal,¹⁴ indicating high quality of the multilayer PtTe₂ and showing its potentials to be used in future optoelectronics. The successful growth of monolayer and multilayer PtTe₂ also provides a significant platform for investigating the unique layer-dependent properties of this material.

■ CONCLUSIONS

In summary, we demonstrate the epitaxial growth of monolayer PdTe₂ and patterned PtTe₂ by direct tellurization of Pd(111) and Pt(111) surfaces as confirmed by STM, XPS and LEED measurements. Large-area and high quality PdTe₂ and patterned PtTe₂ monolayer film were grown at temperature of 470 °C and 200 °C, respectively. PdTe₂ exhibits (1×1) lattice while PtTe₂ shows a (2×2) pattern which is formed by well-ordered Te vacancies. Thickness was calculated based on XPS results and monolayer features of the epitaxial-grown films were confirmed. Annealing at low temperature of 100 °C resulted in non-flat surfaces and coexistence of (1×1) and (2×2) PtTe₂ structures was obtained. High quality multilayer PtTe₂ can also be obtained by increasing the amount of deposited Te and potential excitation of plasmons at 0.4 eV of the multilayer PtTe₂ was measured by HREELS. The simple and robust synthesis of large area 2D materials can facilitate exploring new quantum phenomena and developing potential applications in future optoelectronics.

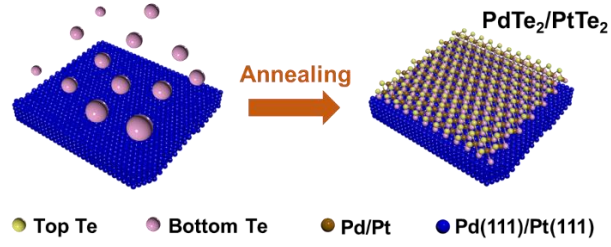


Figure 1. Schematic process of epitaxial growth of monolayer PdTe₂ and patterned PtTe₂ on single crystal Pd (111) or Pt (111) by tellurization.

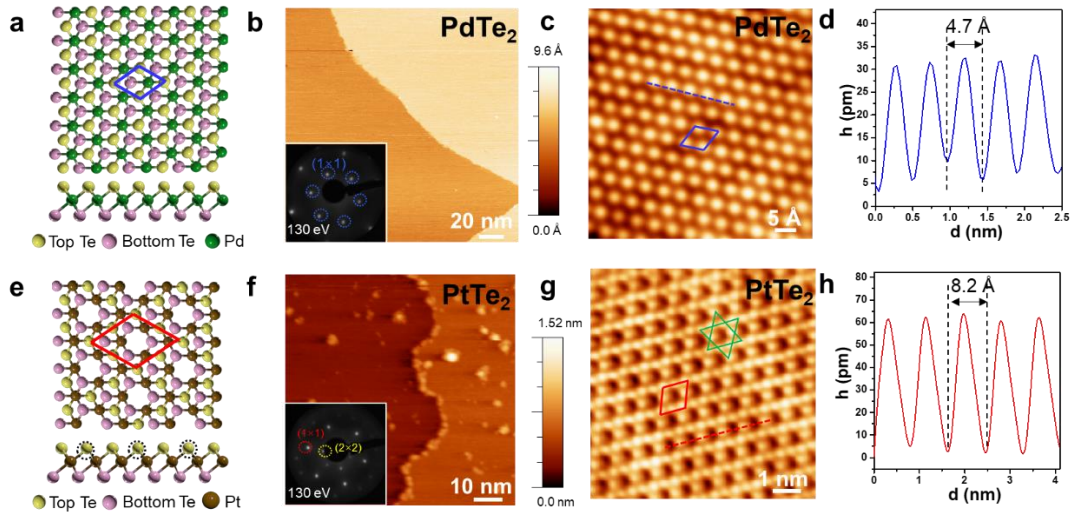


Figure 2. Epitaxial growth of monolayer PdTe₂ and patterned PtTe₂. (a, e) Schematics of atomic structures of as-grown PdTe₂ and patterned PtTe₂, respectively. Top view and side view. Black dashed circles in the side view in (e) indicate missing Te atoms in the atomic row. (b, f) Typical topographic STM images of as-grown PdTe₂ and patterned PtTe₂ films, respectively. Scanning parameters of (b): $V_b = 0.8$ V, $I_t = 0.7$ nA. Scanning parameters of (f): $V_b = -0.5$ V, $I_t = 1.6$ nA. Insets: LEED of PdTe₂ and patterned PtTe₂, respectively. Blue dashed circles indicate the (1×1) PdTe₂ lattice. Red and yellow dashed circles indicate (1×1) and (2×2) lattice of PtTe₂, respectively. (c, g) Atomic resolution STM images of as-grown PdTe₂ and patterned PtTe₂, respectively. Scanning parameters of (c): $V_b = 0.8$ V, $I_t = 0.4$ nA. Scanning parameters of (g): $V_b = -0.5$ V, $I_t = 0.7$ nA. (d, h) Line profiles of PdTe₂ and patterned PtTe₂ corresponding to the blue and red dashed lines in (c) and (g), respectively. Blue rhombuses in (a) and (c) represent unit cells of PdTe₂. Red rhombuses in (e) and (g) represent unit cells of patterned PtTe₂. Green triangles in (g) represent Kagome lattice in the patterned PtTe₂.

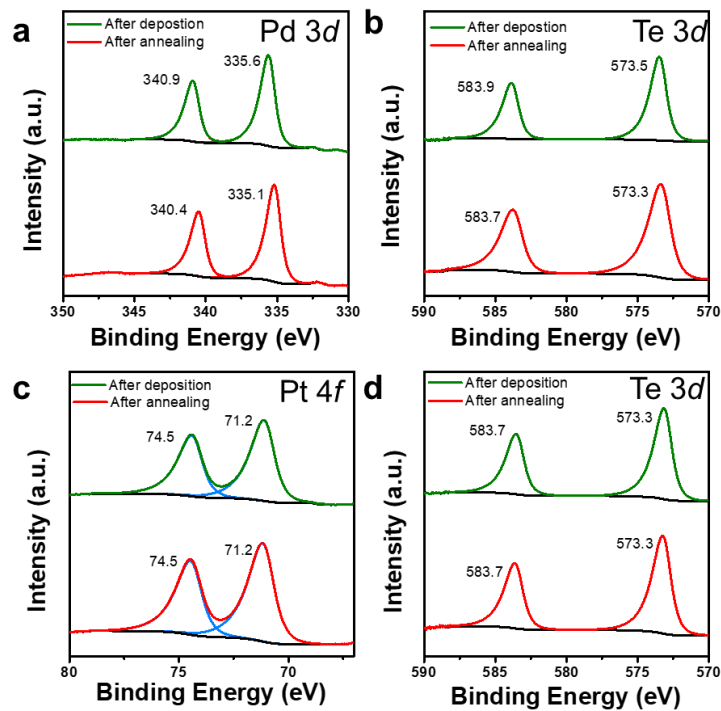


Figure 3. XPS spectra of as-grown PdTe₂ and patterned PtTe₂. (a, b) XPS spectra of Pd 3*d* and Te 3*d* peaks obtained after deposition of Te (green spectra) and following annealing at 470 °C (red spectra), respectively. (c, d) XPS spectra of Pt 4*f* and Te 3*d* peaks obtained after deposition of Te (green spectra) and following annealing at 200 °C (red spectra), respectively.

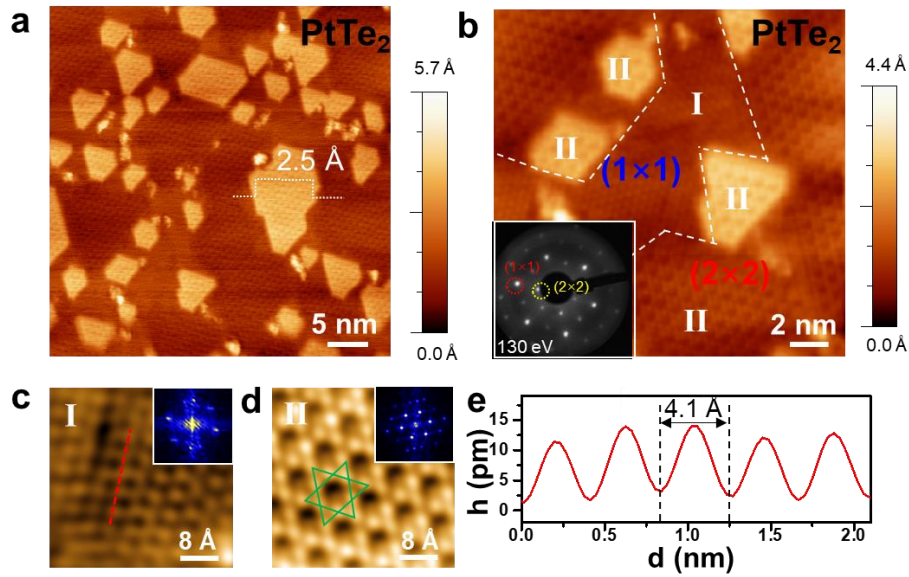


Figure 4. Monolayer patterned PtTe₂ obtained at low annealing temperature of 100°C. (a) A typical STM topographic image of PtTe₂. (b) A zoom-in STM image of (a). Structure I, e.g., confined by white dashed lines, exists only outside the islands. Structure II exists both inside and outside the islands. Inset: LEED patterns of the structure. Red and yellow circles indicate (1×1) and (2×2) lattices, respectively. (c, d) Atomic resolution STM images of (1×1) and (2×2) PtTe₂ structures, respectively. Greens triangles in (d) show the Kagome lattice. Insets of (c) and (d): Fast Fourier Transform (FFT) of each image, respectively. (e) A line profile corresponding to the red dashed line in (c). $V_b = -1.1$ V, $I_t = 0.9$ nA.

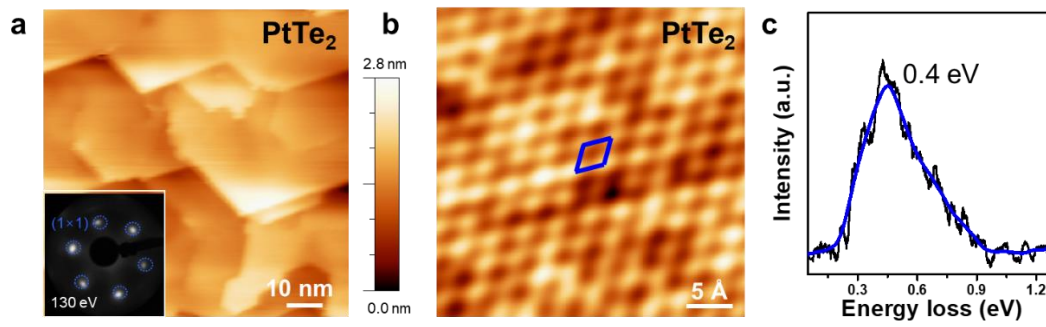


Figure 5. Multilayer PtTe₂ grown by this method. (a) A STM topographic image of multilayer PtTe₂. $V_b = -1.1$ V, $I_t = 0.8$ nA. Inset: LEED patterns of the multilayer PtTe₂. Blue dashed circles indicate (1×1) lattice. (b) An atomic resolution STM image of the multilayer PtTe₂. The blue rhombus indicates a unit cell. $V_b = 0.9$ V, $I_t = 0.7$ nA. (c) A HREELS spectrum of the multilayer PtTe₂ (after background subtraction). The blue line guides the eye. The kinetic energy of the elastic electron beam is 5 eV.

■ ASSOCIATED CONTENT

Supporting Information.

The Supporting Information is available free of charge at XXX

Experimental methods and supplementary figures (PDF)

■ AUTHOR INFORMATION

Corresponding Authors

Yong P Chen - *Department of Physics and Astronomy, Purdue University, West Lafayette, Indiana 47907, USA*; Email: liu2815@purdue.edu; Email: yongchen@purdue.edu

Dmitry Zemlyanov - *Birck Nanotechnology Center, Purdue University, West Lafayette, Indiana 47907, USA*; Email: dzemlian@purdue.edu

Authors

Lina Liu - *Department of Physics and Astronomy, Purdue University, West Lafayette, Indiana 47907, USA*

Author Contributions

Y.C., D.Z. and L.L. conceived the experiments. L.L. and D.Z. conducted the experiments. L.L. analyzed the data and all authors discussed. L.L. wrote the paper. All authors discussed and commented on the manuscript.

Notes

The authors declare no conflict of interest.

■ ACKNOWLEDGMENTS

We acknowledge the partial financial support by the U.S. Department of Energy (Office of Basic Energy Sciences) under Award No. DE-SC0019215. We thank Prof. Ronald G. Reifengerger for fruitful discussions. We express our gratitude to the Center for Nanoscale Materials for the help with the STM tip preparation (use of the Center for Nanoscale Materials, an Office of Science user facility, was supported by the U.S. Department of Energy, Office of Science, Office of Basic Energy Sciences, under Contract No. DE-AC02-06CH11357).

■ REFERENCES

- (1) Pi, L.; Li, L.; Liu, K.; Zhang, Q.; Li, H.; Zhai, T. Recent Progress on 2D Noble-Transition-Metal Dichalcogenides. *Adv. Funct. Mater.* **2019**, *29* (51), 1904932.
- (2) Ciarrocchi, A.; Avsar, A.; Ovchinnikov, D.; Kis, A. Thickness-Modulated Metal-to-Semiconductor Transformation in a Transition Metal Dichalcogenide. *Nat. Commun.* **2018**, *9*, 919.
- (3) Oyedele, A. D.; Yang, S.; Feng, T.; Haglund, A. V.; Gu, Y.; Poretzky, A. A.; Briggs, D.; Rouleau, C. M.; Chisholm, M. F.; Unocic, R. R.; Mandrus, D.; Meyer, III, H. M.; Pantelides, S. T.; Geohegan, D. B.; Xiao, K. Defect-Mediated Phase Transformation in Anisotropic Two-Dimensional PdSe₂ Crystals for Seamless Electrical Contacts. *J. Am. Chem. Soc.* **2019**, *141* (22), 8928-8936.
- (4) Jiang, S.; Xie, C.; Gu, Y.; Zhang, Q.; Wu, X.; Sun, Y.; Li, W.; Shi, Y.; Zhao, L.; Pan, S.; Yang, P.; Huan, Y.; Xie, D.; Zhang, Q.; Liu, X.; Zou, X.; Gu, L.; Zhang, Y.

Anisotropic Growth and Scanning Tunneling Microscopy Identification of Ultrathin Even-Layered PdSe₂ Ribbons. *Small* **2019**, *15* (45), 1902789.

(5) Avsar, A.; Ciarrocchi, A.; Pizzochero, M.; Unuchek, D.; Yazyev, O. V.; Kis, A. Defect Induced, Layer-Modulated Magnetism in Ultrathin Metallic PtSe₂. *Nat. Nanotechnol.* **2019**, *14* (7), 674-678.

(6) Okogbue, E.; Ko, T. J.; Han, S. S.; Shawkat, M. S.; Wang, M.; Chung, H. S.; Oh, K. H.; Jung, Y. Wafer-Scale 2D PtTe₂ Layers for High-Efficiency Mechanically Flexible Electro-Thermal Smart Window Applications. *Nanoscale* **2020**, *12* (19), 10647-10655.

(7) Yu, X.; Yu, P.; Wu, D.; Singh, B.; Zeng, Q.; Lin, H.; Zhou, W.; Lin, J.; Suenaga, K.; Liu, Z.; Wang, Q. J. Atomically Thin Noble Metal Dichalcogenide: a Broadband Mid-Infrared Semiconductor. *Nat. Commun.* **2018**, *9*, 1545.

(8) Hu, D.; Zhao, T.; Ping, X.; Zheng, H.; Xing, L.; Liu, X.; Zheng, J.; Sun, L.; Gu, L.; Tao, C.; Wang, D.; Jiao, L. Unveiling the Layer-Dependent Catalytic Activity of PtSe₂ Atomic Crystals for the Hydrogen Evolution Reaction. *Angew. Chem. Int. Ed.* **2019**, *58* (21), 6977-6981.

(9) Chia, X.; Adriano, A.; Lazar, P.; Sofer, Z.; Luxa, J.; Pumera, M. Layered Platinum Dichalcogenides (PtS₂, PtSe₂, and PtTe₂) Electrocatalysis: Monotonic Dependence on the Chalcogen Size. *Adv. Funct. Mater.* **2016**, *26* (24), 4306-4318.

(10) Clark, O. J.; Neat, M. J.; Okawa, K.; Bawden, L.; Markovic, I.; Mazzola, F.; Feng, J.; Sunko, V.; Riley, J. M.; Meevasana, W.; Fujii, J.; Vobornik, I.; Kim, T. K.; Hoesch, M.; Sasagawa, T.; Wahl, P.; Bahramy, M. S.; King, P. D. C. Fermiology and Superconductivity of Topological Surface States in PdTe₂. *Phys. Rev. Lett.* **2018**, *120* (15), 156401.

(11) Timmons, E. I.; Teknowijoyo, S.; Kończykowski, M.; Cavani, O.; Tanatar, M. A.; Ghimire, S.; Cho, K.; Lee, Y.; Ke, L.; Jo, N. H.; Bud'ko, S. L.; Canfield, P. C.; Orth, P. P.; Scheurer, M. S.; Prozorov, R. Electron Irradiation Effects on Superconductivity in PdTe₂: an Application of a Generalized Anderson Theorem. *Phys. Rev. Res.* **2020**, *2* (2), 023140.

(12) Xue, H.; Yang, H.; Wu, Y.; Yao, G.; Guan, D.; Wang, S.; Zheng, H.; Liu, C.; Li, Y.; Jia, J. Molecular Beam Epitaxy of Superconducting PdTe₂ Films on Topological Insulator Bi₂Te₃. *Science China Physics, Mechanics & Astronomy* **2019**, *62* (7), 076801.

(13) Wang, M. X.; Liu, C.; Xu, J. P.; Yang, F.; Miao, L.; Yao, M. Y.; Gao, C. L.; Shen, C.; Ma, X.; Chen, X.; Xu, Z. A.; Liu, Y.; Zhang, S. C.; Qian, D.; Jia, J. F.; Xue, Q. K. The Coexistence of Superconductivity and Topological Order in the Bi₂Se₃ Thin Films. *Science* **2012**, *336* (6077), 52-55.

(14) Politano, A.; Chiarello, G.; Ghosh, B.; Sadhukhan, K.; Kuo, C. N.; Lue, C. S.; Pellegrini, V.; Agarwal, A. 3D Dirac Plasmons in the Type-II Dirac Semimetal PtTe₂. *Phys. Rev. Lett.* **2018**, *121* (8), 086804.

(15) Yan, M.; Huang, H.; Zhang, K.; Wang, E.; Yao, W.; Deng, K.; Wan, G.; Zhang, H.; Arita, M.; Yang, H.; Sun, Z.; Yao, H.; Wu, Y.; Fan, S.; Duan, W.; Zhou, S. Lorentz-Violating Type-II Dirac Fermions in Transition Metal Dichalcogenide PtTe₂. *Nat. Commun.* **2017**, *8*, 257.

(16) Zeng, L.; Wu, D.; Jie, J.; Ren, X.; Hu, X.; Lau, S. P.; Chai, Y.; Tsang, Y. H. Van der Waals Epitaxial Growth of Mosaic-Like 2D Platinum Ditelluride Layers for Room-Temperature Mid-Infrared Photodetection up to 10.6 μm. *Adv. Mater.* **2020**, *32*, 2004412.

- (17) Villaos, R. A. B.; Crisostomo, C. P.; Huang, Z. Q.; Huang, S. M.; Padama, A. A. B.; Albao, M. A.; Lin, H.; Chuang, F. C. Thickness Dependent Electronic Properties of Pt Dichalcogenides. *npj 2D Mater. Appl.* **2019**, *3* (1), 2.
- (18) Yang, H.; Kim, S. W.; Chhowalla, M.; Lee, Y. H. Structural and Quantum-State Phase Transitions in van der Waals Layered Materials. *Nat. Phys.* **2017**, *13* (10), 931-937.
- (19) Li, E.; Zhang, R. Z.; Li, H.; Liu, C.; Li, G.; Wang, J. O.; Qian, T.; Ding, H.; Zhang, Y. Y.; Du, S. X.; Lin, X.; Gao, H. J. High Quality PdTe₂ Thin Films Grown by Molecular Beam Epitaxy. *Chin. Phys. B* **2018**, *27* (8), 086804.
- (20) Ma, H.; Chen, P.; Li, B.; Li, J.; Ai, R.; Zhang, Z.; Sun, G.; Yao, K.; Lin, Z.; Zhao, B.; Wu, R.; Tang, X.; Duan, X.; Duan, X. Thickness-Tunable Synthesis of Ultrathin Type-II Dirac Semimetal PtTe₂ Single Crystals and Their Thickness-Dependent Electronic Properties. *Nano Lett.* **2018**, *18* (6), 3523-3529.
- (21) Fu, L.; Hu, D.; Mendes, R. G.; Rummeli, M. H.; Dai, Q.; Wu, B.; Fu, L.; Liu, Y. Highly Organized Epitaxy of Dirac Semimetallic PtTe₂ Crystals with Extrahigh Conductivity and Visible Surface Plasmons at Edges. *ACS Nano* **2018**, *12* (9), 9405-9411.
- (22) Lin, X.; Lu, J. C.; Shao, Y.; Zhang, Y. Y.; Wu, X.; Pan, J. B.; Gao, L.; Zhu, S. Y.; Qian, K.; Zhang, Y. F.; Bao, D. L.; Li, L. F.; Wang, Y. Q.; Liu, Z. L.; Sun, J. T.; Lei, T.; Liu, C.; Wang, J. O.; Ibrahim, K.; Leonard, D. N.; Zhou, W.; Guo, H. M.; Wang, Y. L.; Du, S. X.; Pantelides, S. T.; Gao, H. J. Intrinsically Patterned Two-Dimensional Materials for Selective Adsorption of Molecules and Nanoclusters. *Nat. Mater.* **2017**, *16* (7), 717-721.
- (23) Galeev, T. K.; Bulgakov, N. N.; Savelieva, G. A.; Popova, N. M. Surface Properties of Platinum and Palladium. *React. Kinet. Catal. Lett.* **1980**, *14* (1), 61-65.
- (24) Smith, K. C.; Saenz, D. A.; Zemlyanov, D. Y.; Voevodin, A. XPS Thickness Solver. <https://nanohub.org/resources/xpsts/> (accessed Sep 15, 2014).
- (25) Gharachorlou, A.; Detwiler, M. D.; Nartova, A. V.; Lei, Y.; Lu, J.; Elam, J. W.; Delgass, W. N.; Ribeiro, F. H.; Zemlyanov, D. Y. Palladium Nanoparticle Formation on TiO₂(110) by Thermal Decomposition of Palladium(II) Hexafluoroacetylacetonate. *ACS Appl. Mater. Inter.* **2014**, *6* (16), 14702-14711.
- (26) Zemlyanov, D. Y.; Jespersen, M.; Zakharov, D. N.; Hu, J. J.; Paul, R.; Kumar, A.; Pacley, S.; Glavin, N.; Saenz, D.; Smith, K. C.; Fisher, T. S.; Voevodin, A. A. Versatile Technique for Assessing Thickness of 2D Layered Materials by XPS. *Nanotechnology* **2018**, *29* (11), 115705.
- (27) Electron Spectroscopy: Theory, Techniques and Applications. Fadley, C. S. Academic Press, London New York, USA 1977.
- (28) Scofield, J. H. Hartree-Slater Subshell Photoionization Cross Sections at 1254 and 1487 eV. *J. Electron. Spectrosc.* **1976**, *8* (2), 129-137.
- (29) Yeh, J. J.; Lindau, I. Atomic Subshell Photoionization Cross Sections and Asymmetry Parameters: $1 \leq Z \leq 103$. *At. Data Nucl. Data Tables* **1985**, *32* (1), 1-155.
- (30) Powell, C. J.; Jablonski, A. NIST Electron Effective-Attenuation-Length Database, Version 1.3; National Institute of Standards and Technology: Gaithersburg, MD, 2011.
- (31) Wang, Y.; Li, L.; Yao, W.; Song, S.; Sun, J. T.; Pan, J.; Ren, X.; Li, C.; Okunishi, E.; Wang, Y. Q.; Wang, E.; Shao, Y.; Zhang, Y. Y.; Yang, H. T.; Schwier, E. F.; Iwasawa, H.; Shimada, K.; Taniguchi, M.; Cheng, Z.; Zhou, S.; Du, S.; Pennycook, S. J.; Pantelides, S. T.; Gao, H. J. Monolayer PtSe₂, a New Semiconducting Transition-Metal-Dichalcogenide, Epitaxially Grown by Direct Selenization of Pt. *Nano Lett.* **2015**, *15* (6), 4013-4018.

(32) Xiong, W.; Huang, K.; Yuan, S. The Mechanical, Electronic and Optical Properties of Two-Dimensional Transition Metal Chalcogenides MX_2 and M_2X_3 (M = Ni, Pd; X = S, Se, Te) with Hexagonal and Orthorhombic Structures. *J. Mater. Chem. C* **2019**, 7 (43), 13518-13525.

(32) Michaelson, H. B. The Work Function of the Elements and its Periodicity. *J. Appl. Phys.* **1977**, 48 (11), 4729-4733.

(34) Hao, S.; Zeng, J.; Xu, T.; Cong, X.; Wang, C.; Wu, C.; Wang, Y.; Liu, X.; Cao, T.; Su, G.; Jia, L.; Wu, Z.; Lin, Q.; Zhang, L.; Yan, S.; Guo, M.; Wang, Z.; Tan, P.; Sun, L.; Ni, Z.; Liang, S. J.; Cui, X.; Miao, F. Low-Temperature Eutectic Synthesis of PtTe_2 with Weak Antilocalization and Controlled Layer Thinning. *Adv. Funct. Mater.* **2018**, 28 (36). 1803746.

Supporting Information

Epitaxial Growth of Monolayer PdTe₂ and Patterned PtTe₂ by Direct Tellurization of Pd and Pt surfaces

Lina Liu,[†] Dmitry Zemlyanov,^{*,○} and Yong P. Chen^{*,†,○,§,||,⊥}

[†]Department of Physics and Astronomy, Purdue University, West Lafayette, Indiana 47907, USA

[○]Birck Nanotechnology Center, Purdue University, West Lafayette, Indiana 47907, USA

[§]Purdue Quantum Science and Engineering Institute and School of Electrical and Computer Engineering, Purdue University, West Lafayette, Indiana 47907, USA

^{||}WPI-AIMR International Research Center on Materials Sciences, Tohoku University, Sendai 980-8577, Japan

[⊥]Institute of Physics and Astronomy and Villum Centers for Dirac Materials and for Hybrid Quantum Materials and Devices, Aarhus University, 8000 Aarhus-C, Denmark

1. Experimental details

(1) Epitaxial growth of PdTe₂ and patternedPtTe₂ on Pd(111) and Pt(111)

All experiments were performed with an Omicron Surface Analysis Cluster. The system, as described elsewhere,¹⁻³ consists of an ultrahigh vacuum (UHV) preparation chamber and UHV μ -metal analysis chamber with base pressures of 1×10^{-9} mbar and 5×10^{-11} mbar, respectively. Pd(111) and Pt(111) single crystals with ~ 9 mm of diameter, 1 mm of thickness and with orientation accuracy $< 0.5^\circ$ (MaTeck GmbH) were cleaned by repeated cycles of Ar⁺ sputtering and annealing in UHV at 780 °C. The surface cleanliness was monitored by XPS, LEED, and STM. Tellurium (99.999%, Sigma-Aldrich) was thermally evaporated using a home-built evaporator in the preparation chamber. The tellurium evaporation temperature was in the range of 290-300°C and the evaporation rate was controlled by the heater power. The amount of deposited tellurium was verified by XPS. The substrate was kept at room temperature during deposition. The sample temperature was measured by a K-type thermocouple attached to the manipulator part with which a sample holder was in a good thermal contact. For each experiment, the single crystal was freshly cleaned and Te was deposited at room temperature. Then the sample was annealed at the specified temperature for 10 mins in UHV.

(2) STM, XPS and LEED measurements

STM images (Omicron ambient temperature UHV STM) were collected at room temperature using electrochemically etched W and Pt-Ir tips at constant current (topographic) mode. In all experiments reported here, the tip was electrically grounded, meaning that at positive bias the current flowed from sample to tip. The STM images were analyzed using WSxM software.⁴

XPS was acquired using a non-monochromatic Mg K α X-ray source ($h\nu = 1253.6$ eV) at 150 W. High resolution spectra were recorded at constant pass energy of 20 eV using the electron energy analyzer-Omicron EAC 125 and the analyzer controller-Omicron EAC 2000. The resolution of the instrument, which was measured as the full width at half maximum (FWHM) of Pt 4f_{7/2} peaks of the clean Pt(111) crystal, was approximately 1.2 eV. Photoelectrons were collected at a 45° angle with respect to the surface normal. Pt 4f peaks of Pt(111) were used for XPS quantification in this study. The density, kinetic energy and asymmetry parameter are 21.4 g·cm⁻³, 1182.4 eV and

1.02, respectively. The calculated inelastic mean free path, transport mean free path and practical electron attenuation length (EAL) for a film thickness of 10 Å are 14.75 Å, 25.03 Å and 10.71 Å, respectively.⁵

LEED measurements were conducted in the analyst chamber straight after sample preparation with a four-grid detector (Omicron LEED spectra).

2. LEED measurements of as-grown PdTe₂

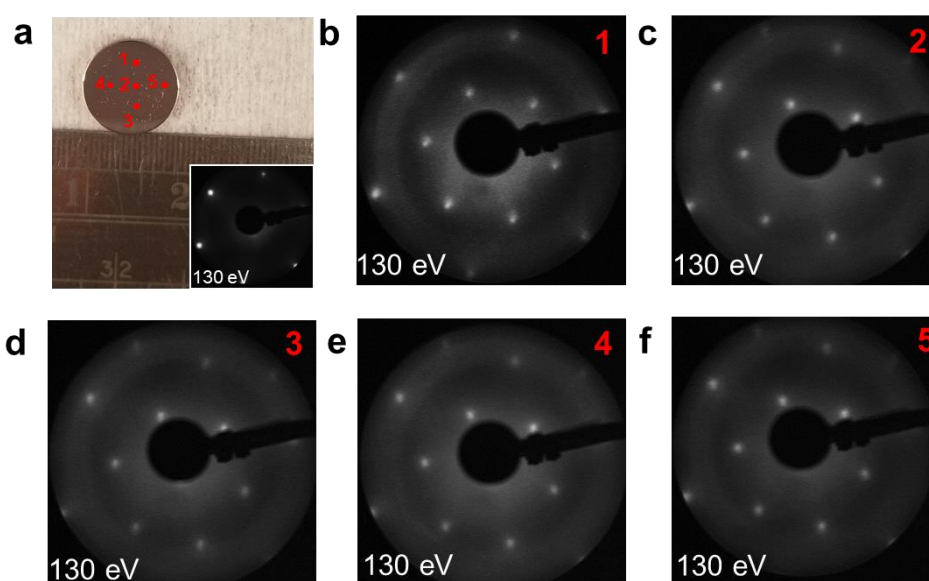


Figure S1. LEED measurements at different positions of the crystal. (a) A photo of the Pd(111) single crystal used in this study with a monolayer PdTe₂ grown on the surface. For comparison, LEED of clean Pd(111) is shown in the inset. (b-f) LEED measurements corresponding to different spots on the crystal numbered 1-5 in (a). Approximately a surface area size of ~6 mm was characterized, indicating a large PdTe₂ film grown on the surface.

3. Thermal stability of the (2×2) PtTe₂ pattern

After annealing in UHV at 500 °C, LEED results of the (2×2) PtTe₂ pattern did not change (Figure S2a), indicating the high thermal stability of the structure. However, additional defects were observed in the detailed STM images (Figure S2b and S2c). A vacancy defect which contains one Pt atom and three Te atoms (V_{1Pt3Te}) was observed (Figure S2c and S2d), indicating that further missing of atoms took place locally during high temperature annealing.

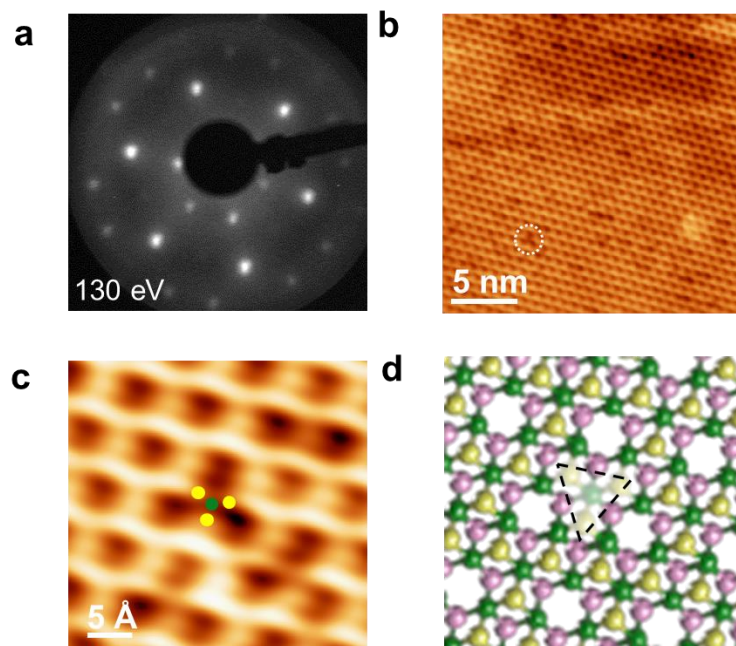


Figure S2. Thermal stability of the (2×2) PtTe_2 pattern. (a) LEED measurement of the (2×2) PtTe_2 pattern following annealing at 500°C in UHV. (b) A detailed STM image of the (2×2) PtTe_2 pattern following annealing at 500°C in UHV. A vacancy defect of $\text{V}_{1\text{Pt}3\text{Te}}$ is marked by the white dashed circle. (c, d) A zoom-in STM image and schematic image of the $\text{V}_{1\text{Pt}3\text{Te}}$ defect in (b), respectively. Pt and Te atoms in (c) are shown by green and yellow dots, respectively. The $\text{V}_{1\text{Pt}3\text{Te}}$ defect is marked by a black dashed triangle in (d). $V_b = -1.1\text{ V}$, $I_t = 0.9\text{ nA}$.

4. XPS spectra of clean Pd(111) and Pt(111)

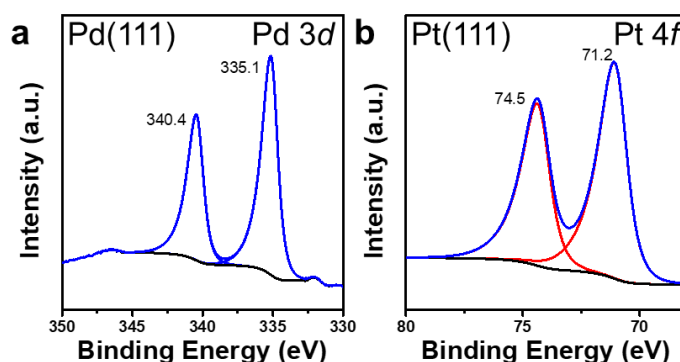


Figure S3. (a, b) XPS Pd $3d$ and Pt $4f$ spectra obtained on clean Pd(111) and Pt(111), respectively.

5. STM images of PdTe_2 obtained at low temperature and clean Pd(111)

The STM image of clean Pd(111) exhibits flat and large terraces with the width of tens of nanometers (Figure S4b), which is dramatically different from the small and irregular islands after the growth of PdTe_2 in Figure S4a, indicating breaking apart of terraces

and mass-transport during growth.

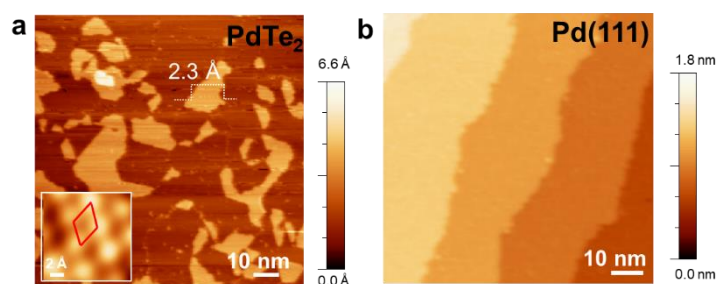


Figure S4. (a) A typical STM topographic image of PdTe₂ obtained at 100 °C. Inset: Atomic resolution STM image of PdTe₂. The red rhombus represents a unit cell. $V_b = -1.3$ V, $I_t = 0.6$ nA. A typical STM topographic image of clean Pd(111). $V_b = -0.9$ V, $I_t = 0.7$ nA

6. XPS characterizations of multilayer PtTe₂

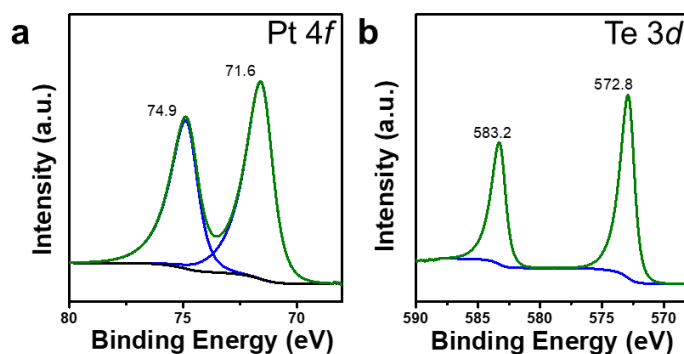


Figure S5. XPS spectra of multilayer PtTe₂. (a, b) Pt 4f and Te 3d peaks of multilayer PtTe₂, respectively.

References

- (1) Paul, R.; Reifenberger, R. G.; Fisher, T. S.; Zemlyanov, D. Y. Atomic Layer Deposition of FeO on Pt(111) by Ferrocene Adsorption and Oxidation. *Chem. Mater.* **2015**, *27* (17), 5915-5924.
- (2) Gharachorlou, A.; Detwiler, M. D.; Mayr, L.; Gu, X. K.; Greeley, J.; Reifenberger, R. G.; Delgass, W. N.; Ribeiro, F. H.; Zemlyanov, D. Y. Surface Chemistry of Trimethylaluminum on Pd(111) and Pt(111). *J. Phys. Chem. C* **2015**, *119* (33), 19059-19072.
- (3) Gharachorlou, A.; Detwiler, M. D.; Nartova, A. V.; Lei, Y.; Lu, J.; Elam, J. W.; Delgass, W. N.; Ribeiro, F. H.; Zemlyanov, D. Y. Palladium Nanoparticle Formation on TiO₂(110) by Thermal Decomposition of Palladium(II) Hexafluoroacetylacetonate. *ACS Appl. Mater. Inter.* **2014**, *6* (16), 14702-14711.

(4) Horcas, I.; Fernandez, R.; Gomez-Rodriguez, J. M.; Colchero, J.; Gomez-Herrero, J.; Baro, A. M. WSXM: a Software for Scanning Probe Microscopy and a Tool for Nanotechnology. *Rev. Sci. Instrum.* **2007**, *78* (1), 013705.

(5) Powell, C. J.; Jablonski, A. NIST Electron Effective-Absorption-Length Database, Version 1.3; National Institute of Standards and Technology: Gaithersburg, MD, 2011.